

# Observation and modeling of the evolution of Texas power plant plumes

W. Zhou<sup>1</sup>, D. S. Cohan<sup>1</sup>, R. W. Pinder<sup>2</sup>, J. A. Neuman<sup>3, 4</sup>, J. S. Holloway<sup>3, 4</sup>, J. Peischl<sup>3, 4</sup>, T. B. Ryerson<sup>3</sup>, J. B. Nowak<sup>3,4</sup>, F. Flocke<sup>5</sup>, W. G. Zheng<sup>5</sup>

[1]{Department of Civil and Environmental Engineering, Rice University, Houston, Texas}

[2]{Office of Research and Development, US Environmental Protection Agency, North Carolina, USA}

[3]{Chemical Sciences Division, Earth System Research Laboratory, NOAA, Boulder, Colorado, USA}

[4]{Cooperative Institute for Research in Environmental Sciences, University of Colorado, Boulder, Colorado, USA}

[5]{National Center for Atmospheric Research, Boulder, Colorado, USA}

Correspondence to: W. Zhou (zhouwei@rice.edu)

## Abstract

During the second Texas Air Quality Study 2006 (TexAQS II), a full range of pollutants was measured by aircraft in eastern Texas during successive transects of power plant plumes (PPPs). A regional photochemical model is applied to simulate the physical and chemical evolution of the plumes. The observations reveal that SO<sub>2</sub> and NO<sub>y</sub> were rapidly removed from PPPs on a cloudy day but not on the cloud-free days, indicating efficient aqueous processing of these compounds in clouds. The model reasonably represents observed NO<sub>x</sub> oxidation and PAN formation in the plumes, but fails to capture the rapid loss of SO<sub>2</sub> (0.37 hour<sup>-1</sup>) and NO<sub>y</sub> (0.24 hour<sup>-1</sup>) in some plumes on the cloudy day. Adjustments to the cloud liquid water content (QC)

and the default metal concentrations in the cloud module could explain some of the SO<sub>2</sub> loss. However, NO<sub>y</sub> in the model was insensitive to QC. These findings highlight cloud processing as a major challenge to atmospheric models. Model-based estimates of ozone production efficiency (OPE) in PPPs are 20-50% lower than observation-based estimates for the cloudy day.

## **1 Introduction**

Power plants are the leading point source emitters of SO<sub>2</sub> and oxides of nitrogen (NO<sub>x</sub>=NO+NO<sub>2</sub>) (EPA, 2009). The large amount of SO<sub>2</sub> and NO<sub>x</sub> emitted from power plants has been linked to a series of environmental issues, such as acid deposition, photochemical O<sub>3</sub> and particulate matter (Srivastava et al., 2004; Ryerson et al., 2001; Brock et al., 2003; Flues et al., 2002). Various regulations and market-based policies have been implemented to reduce these emissions, including the Acid Rain Program (EPA, 2005) and the NO<sub>x</sub> State Implementation Plan Call (NO<sub>x</sub> SIP Call) (EPA, 2004) in the United States. Power plants are among the most accurately measured emission sources in the U.S. national emission inventory due to direct smoke stack measurements by Continuous Emission Monitoring Systems (CEMS). Good agreement has been found in comparing power plant emissions reported by CEMS with airborne measurements of power plant plumes (PPPs) (Frost et al., 2006) and with satellite measurements of NO<sub>2</sub> (Kim et al., 2006).

The emissions, transport, and chemical evolution of pollutants from power plants have been investigated by multiple observational and modeling methods (Ryerson et al., 1998; Neuman et al., 2004; Godowitch et al., 2008a; Frost et al., 2006; Kim et al., 2006; Sillman, 2000). Airborne measurement of chemical composition and meteorological parameters in PPP transects have

1 been conducted in several field campaigns over North America (Trainer et al., 1995; Ryerson et  
2 al., 1998; Springston et al., 2005; Neuman et al., 2009).

3 SO<sub>2</sub> freshly emitted from power plant stacks is quickly diluted and undergoes chemical  
4 evolution during plume transport. Previous aircraft measurements in PPPs have revealed that  
5 gas-phase SO<sub>2</sub> oxidation is the key pathway for the SO<sub>2</sub> removal and the particle growth in PPPs  
6 in the absence of clouds (Brock et al., 2002, 2003; Springston et al., 2005). SO<sub>2</sub> can also readily  
7 dissolve in cloud water and then convert to sulfate via aqueous reactions.

8 Several previous field studies have investigated the chemical evolution and lifetime of NO<sub>x</sub>,  
9 ozone production efficiency, and the loss rate of reactive nitrogen in PPPs (Ryerson et al., 1998;  
10 Springston et al., 2005; Neuman et al., 2009). Some studies have reported the rapid loss of NO<sub>y</sub>  
11 in PPPs which they primarily attributed to HNO<sub>3</sub> loss (Neuman et al., 2004; Nunnermacker et al.,  
12 2000), but others have not (Ryerson et al., 2003).

13 Power plants are significant contributors to NO<sub>x</sub> and SO<sub>2</sub> emissions and high ozone  
14 concentrations in eastern Texas. A NOAA WP-3 aircraft performed successive downwind  
15 transects of PPPs in this region during several flights as part of the summer 2006 Second Texas  
16 Air Quality Study (TexAQS II) (Parrish et al., 2009). The instruments aboard the WP-3  
17 measured a full range of trace gases, aerosol parameters, and meteorological parameters at high  
18 time resolution and spatial resolution. This study utilizes the rich data source to examine whether  
19 a 3D photochemical model with a fine spatial resolution but without subgrid plume treatment can  
20 effectively simulate the chemical and physical evolution of PPPs as they disperse and transport  
21 downwind. We focus on the evolution of sulfur, reactive nitrogen, and O<sub>3</sub> in the plumes.

22

## **2 Airborne measurement**

TexAQS II was a comprehensive observational campaign in eastern Texas from August to October, 2006, which aimed to improve scientific understanding of the sources and atmospheric processes responsible for the formation and distribution of O<sub>3</sub> and aerosols in the region (Parrish et al., 2009). PPPs observed during TexAQS II originated from eastern Texas coal-fired power plants with a large range of reported NO<sub>x</sub> and SO<sub>2</sub> emission rates (Table 1 and Fig. 1).

The measurements and operational characteristics of the NOAA WP-3 have been summarized elsewhere (Parrish et al., 2009). Instruments aboard the WP-3 measured numerous reactive nitrogen species (NO, NO<sub>2</sub>, HNO<sub>3</sub>, NO<sub>3</sub>, N<sub>2</sub>O<sub>5</sub>, PAN, peroxy propionyl nitrate, methacryloyl peroxy nitrate), isoprene, CO<sub>2</sub>, CO, SO<sub>2</sub>, HCHO, major aerosol parameters, UV-VIS actinic flux, relative humidity, and temperature (Tables A1a and A1b of Parrish et al. (2009) and the references therein). The instruments used in measuring major gas-phase species are summarized in Table S2 (in supplementary materials). The time resolution of most instruments was 1 second, equal to approximately 100m spatial resolution at typical WP-3 flying speeds.

Coal-fired power plants are major sources of SO<sub>2</sub> and NO<sub>x</sub>, so their plumes can be identified by elevated concentrations of SO<sub>2</sub> and NO<sub>y</sub> (Ryerson et al., 1998; Ryerson et al., 2003). SO<sub>2</sub> enhancement can be a more reliable diagnostic of PPPs than NO<sub>y</sub> since there are numerous sources of NO<sub>x</sub>, but coal-fired power plants are dominant sources of SO<sub>2</sub> in eastern Texas (Ryerson et al., 2003; Neuman et al., 2009). Background SO<sub>2</sub> levels were consistently below 1 ppb, so this level of SO<sub>2</sub> is chosen as a threshold value for identifying PPPs.

In rural areas of northeastern Texas, power plants are also leading sources of CO and anthropogenic CO<sub>2</sub> (Nicks et al., 2003), even though CO is not strongly elevated in all PPPs. Airborne measurements in 2000 and 2006 showed that CO and CO<sub>2</sub> could be signatures of the

1 Martin Lake, Monticello, and Welsh plumes, the concentration enhancements of which  
2 completely overlap SO<sub>2</sub> and NO<sub>y</sub> concentration enhancements at transects (Nicks et al., 2003).  
3 As the atmospheric lifetime of CO<sub>2</sub> is years, it is a conservative species in plumes. CO has a  
4 lifetime of one to two months in the atmosphere (Akimoto, 2003), thus serving as another  
5 conservative species in PPPs. CO emissions from Martin Lake, Monticello, and Big Brown,  
6 which were significantly underestimated in a previous emission inventory (1999), were more  
7 accurately estimated in TexAQS II (Peischl et al., 2010).

8 Of the 18 WP-3 flights during TexAQS II, the 16 September and 25 September flights  
9 measured successive cross-wind transects of PPPs from multiple power plants and the 19  
10 September flight measured the Parish plume (Fig. 1 and Table S3). The 16 September flight  
11 (11:00 to 15:00 local time) observed transects of plumes from the Martin Lake, Pirkey,  
12 Monticello, and Welsh power plants at successive downwind distances (Fig. 2a). Since the three  
13 plumes transported northward through rural areas devoid of other large anthropogenic SO<sub>2</sub>  
14 sources, SO<sub>2</sub> concentration enhancements clearly denote plume locations (Fig. 2a). Pirkey is  
15 located several km north-northeast (downwind) of Martin Lake, so their plumes cannot be  
16 distinguished on this flight after the first Martin Lake transect; we refer to the plume as Martin  
17 Lake (Ma-1) for simplicity. On 19 September, the WP-3 measured five plume transects of Parish  
18 in the Houston-Galveston Brazoria (HGB) metropolitan region. On 25 September (13:00 to  
19 16:00 local time), the WP-3 measured two plume transects of Big Brown and Limestone under  
20 northerly flow, and two plume transects of Parish (Fig. S5 and S6 in supplementary materials).  
21 All transects on the three days occurred at altitudes of 600-700 m, well within the planetary  
22 boundary layer height of approximately 1500 m determined from measured temperature profiles.

The exception was five transects (Ma-4 to Ma-8) of the Martin Lake plume at different heights but at the same downwind distance on 16 September.

### **3 Model setup and input parameters**

Atmospheric chemistry for the episode was simulated by the Community Multiscale Air Quality (CMAQ) model (Byun and Schere, 2006) version 4.7 (Foley et al., 2010), using the CB05 chemical mechanism (Yarwood et al., 2005). Inline processing was applied to generate the meteorology dependent emissions properties (i.e., biogenic emissions) (Foley et al., 2010). After accounting for plume rise, most of the power plant emissions were modeled to be released between 200 and 600 m elevation (Fig. S7).

The model was configured with 34 vertical layers and three one-way nested domains. The outer two domains cover the continental U.S. (148×112 with 36 km grid resolution) and the eastern U.S (279×240 with 12km grid resolution) including all of Texas, respectively. The rectangular frame in Fig. 1 shows the fine domain with 4km grid resolution. A full description of the modeling configuration and performance for the 12km domain can be found in Appel et al. (2009). The CMAQ modeling for the 4km domain was from September 1-25, 2006, which covers the days with WP-3 plume measurements.

Meteorology for the episode was simulated by the Fifth-Generation NCAR/Penn State Mesoscale Model (MM5) (Grell et al., 1994) version 3.7.4 for the 36 km domain. For the inner domains (12km and 4km modeling domains), the Weather Research and Forecasting Model (WRF) version 3.0 (Skamarock et al., 2008) was used because of its lower biases in simulated wind and temperature than MM5. Both models had 34 vertical layers extending from the surface

up to 100 hPa. WRF was applied with Asymmetric Convective Model 2 PBL model (Pleim, 2007), Pleim-Xiu Land Surface Model (Xiu and Pleim, 2001), Dudhia shortwave radiation scheme (Dudhia, 1989), RRTM longwave radiation scheme (Mlawer et al., 1997), Kain-Fritsch 2 subgrid convective scheme (Kain, 2004), and the Thompson microphysics scheme (Thompson et al., 2004). MM5 used similar physical schemes. The consistency between MM5 and WRF for the modeling domains was tested and verified (Appel et al., 2009). Meteorological fields were converted to CMAQ-ready format by MCIP version 3.4.2 (Otte and Pleim, 2009).

Emission inputs for the three modeling domains were generated by the Sparse Matrix Operator Kernel Emissions (SMOKE) model (EPA, 2006) based on the National Emission Inventory for 2005. Mobile emissions were projected to 2006 and actual Continuous Emission Monitoring System (CEMS) data were used for point sources. BEIS3.12 (Environmental Protection Agency Biogenic Emissions Inventory System 3.12) (<http://www.epa.gov/asmdnerl/biogen.html>) was applied to compute the biogenic emissions.

NO<sub>y</sub> species in the CB05 chemical mechanism are NO, NO<sub>2</sub>, NO<sub>3</sub>, N<sub>2</sub>O<sub>5</sub>, HONO, HNO<sub>3</sub>, PNA (peroxynitric acid), PAN (peroxyacetyl nitrate), PANX (C3 and higher peroxyacyl nitrates), and NTR (organic nitrate). The sum of all these species (with N<sub>2</sub>O<sub>5</sub>\*2) is the concentration of NO<sub>y</sub> from the model.

The aqueous processing module in CMAQ (Walcek and Taylor, 1986) processes the absorption of gas-phase species and accumulation-mode aerosols separately. The gas-phase absorption into liquid water content of clouds depends on the thermodynamic equilibrium, whereas accumulation-mode aerosols are assumed to be completely activated to form cloud droplets. The dissociation of compounds into ions, oxidation of S(IV) to S(VI) by aqueous H<sub>2</sub>O<sub>2</sub>, O<sub>3</sub>, Fe(III) and Mn(II) etc, and wet deposition are also processed in the model. For computational

1 efficiency, CMAQ does not transport cloud-aqueous concentrations separately from gas-phase  
2 concentrations between model grids. At the end of the cloud processing module, the cloud  
3 concentrations are removed and the mass of each species is passed to either gas-phase or aerosol  
4 concentrations.

5 In this study, the advection schemes used in processing pollutant transport by CMAQ are  
6 Piecewise Parabolic Method (PPM) (Colella and Woodward, 1984) and Yamartino-Blackman  
7 Cubic Scheme (YAM) (Yamartino, 1993). The Asymmetric Convective Model version 2  
8 (ACM2) (Pleim, 2007) was used to simulate the vertical mixing of pollutants in CMAQ.

9 To identify and analyze the impact of each power plant, a zero-out simulation is run with the  
10 emissions of that facility removed from the base emission inventory. The difference between  
11 concentrations in the base simulation and each zero-out simulation represents the zero-out-  
12 contribution (ZOC) of that power plant.

#### 14 **4 Results and Discussion**

15 During airborne measurement on the three days, ground temperature was 24.4-35.5°C  
16 (average: 29.0 °C) and surface wind was 0-7.2 m/s (average: 3.1m/s) at ground-based monitors  
17 in eastern Texas. At 600-700m above the ground level (WP-3 typical flying height), the observed  
18 ambient temperature was 23.7-30.3°C (average: 26.8 °C), wind speed was 1.6-12.0 m/s (average:  
19 6.4 m/s) and no precipitation was observed. The height of the planetary boundary layer (PBL),  
20 determined from the vertical profiles of equivalent potential temperature for the three days, was  
21 about 1500 m on 16 September and about 1000 m in the HGB region on 19 and 25 September.

The CEMS-reported SO<sub>2</sub> and NO<sub>x</sub> emissions of big power plants in the eastern U.S. were previously evaluated based on with WP-3 measurements of PPPs in 2004 (Frost et al., 2006). Since the emitted NO<sub>x</sub> in PPPs can quickly be oxidized to NO<sub>z</sub> (NO<sub>z</sub> = NO<sub>y</sub>-NO<sub>x</sub>), the observed enhancements of NO<sub>y</sub> and SO<sub>2</sub> serve as the basis for evaluation. The strong correlation between NO<sub>y</sub> and SO<sub>2</sub> for all first plume transects ( $R^2=0.68\sim0.98$ ) suggests that the power plants were the dominant sources of these gases there. The three ratios of these plants show strong consistency within the uncertainties of the measurements, although the model slightly under-predicts SO<sub>2</sub>/NO<sub>y</sub> ratios (Table 2). Likewise, previous studies have reported strong consistency between CEMS(SO<sub>2</sub>/NO<sub>x</sub>) and OBS(SO<sub>2</sub>/NO<sub>y</sub>) (Frost et al., 2006; Ryerson et al., 2003; Ryerson et al., 2001).

#### **4.1 Evaluation of plume dispersion and transport**

On 16 September, the WP-3 observed mostly southerly winds with average wind speeds of 6.9 m/s. The southerly winds allowed PPPs of Monticello and Welsh to remain distinct in both model and observation (Fig. 2) but caused the Martin Lake and Pirkey plumes to coincide since the two plants are just 18.5 km apart. Maximal SO<sub>2</sub> enhancements for each plume transect were used to identify the plume centers to enable comparative analyses of observations and modeling results. The plumes produced by CMAQ mostly have similar spatial extent to the measured plumes on 16 September (Fig. 2), 19 and 25 September (Fig. S5-S6). The wind speed and direction in the model were more homogeneous than observed winds, resulting in slight differences between modeled and observed locations of the plumes and plume centers (Fig. 2).

The high-resolution aircraft observations were compared with the model outputs extracted from the corresponding grid cells, adjusted to align the modeled and measured plume peak

1 locations as necessary. Since the aircraft was flying consistently at approximately 100 m/s at  
2 each plume transect, each gridline interval in Fig. 3 (40 seconds) is equal to the spatial distance  
3 of 4 km (one grid cell).

4 The 16 September flight path proceeded northward in 14 successive crosswind (east-west)  
5 transects, the first 12 of which intercepted the Martin Lake (and Pirkey) plumes (Ma-1 to Ma-12  
6 in Fig. 2; Ma-4 to Ma-8 are increasing altitudes at the same transect) and the last four of which  
7 intercepted the Monticello and Welsh plumes (Fig. 2). The extensive observation of the Martin  
8 Lake plume provides a unique opportunity to examine plume evolution from the emission stack  
9 until dilution to background levels. Comparisons between modeled and observed SO<sub>2</sub>, NO<sub>y</sub>, and  
10 CO mixing ratios are shown for each successive plume transect in Fig. S1- S4.

11 At the first transect of the Martin Lake, Monticello, and Welsh plumes, the model generates  
12 lower peak SO<sub>2</sub> and NO<sub>y</sub> concentrations and wider plumes than was observed. This likely reflects  
13 the inability of the 4-km resolution model to resolve subgrid-scale plume structure in the initial  
14 formation of a plume. No subgrid or Plume-in-Grid (PinG) was used in the modeling.

15 The model captured the observed extent of CO at each plume transect, slightly under-  
16 estimating the peak values (Fig. 3). The modeled SO<sub>2</sub> (18ppb) at Ma-2 matched the observed  
17 peak (23 ppb) closely as subgrid effect weakened and the plume width was larger than one grid  
18 cell. As the plume transported to Ma-3, the modeled SO<sub>2</sub> (14ppb) was higher than the observed  
19 peak (7ppb). The modeled SO<sub>2</sub> at plume center was consistently higher than the observed while  
20 the background SO<sub>2</sub> matched observations.

21 The measured CO at the plume center declined only from 240 (Ma-1) to 150 ppb (Ma-3).  
22 However, SO<sub>2</sub> was observed to decline by more than a factor of 10 from Ma-1 to Ma-3,  
23 indicating rapid loss.

Ma-4 through Ma-8 observed the Martin Lake plume at the same downwind distance (53 km) but flew at different altitudes (Ma-4 to Ma-8 of Fig. S1; Table S3). SO<sub>2</sub> emission from Martin Lake was modeled to occur mostly at 400 m, accounting for the stack height and plume rise (Fig. S7). At 1800 m (Ma-4), which was near the top of the PBL, no enhancement of SO<sub>2</sub>, NO<sub>y</sub>, or CO was simulated but a weak SO<sub>2</sub> plume was observed, implying that the model failed to capture some of the observed upward transport. At lower flight altitudes (between 660 and 300 m, corresponding to Ma-6 to Ma-8 in Fig. S1), the model effectively simulated plume extent. The comparisons between the modeled and observed SO<sub>2</sub>, CO and NO<sub>y</sub> species on 19 and 25 September are shown in Fig.S1 to S4.

## 4.2 Correlations between conservative and non-conservative species

In this section, we explore the correlation between conservative and non-conservative species from the observed plume concentrations. The correlations are presented by the slopes and R<sup>2</sup> of the least-square-fit between conservative and non-conservative species. At the time scale of PPP transport (a few hours), CO and CO<sub>2</sub> are expected to experience similar dispersion and minimal loss to chemistry or deposition, leading to near constant slopes of CO to CO<sub>2</sub>. CO and CO<sub>2</sub> concentrations were strongly correlated within the Martin Lake and Monticello plumes and the slopes of CO to CO<sub>2</sub> held steady as both plumes aged (Fig. 4) (for Ma-1 to Ma-3 and Ma-6 to Ma-12, slopes of the least square fit: 0.58~0.71 ppb/ppm, R<sup>2</sup>: 0.89~0.96; for Mo-1 to Mo-4, slopes of the least square fit: 4.3~5.3 ppb/ppm, R<sup>2</sup>:0.77~0.94), indicating the same extent of dispersion of CO and CO<sub>2</sub>. For the Welsh and Big Brown plumes, only the first one or two transects had a strong correlation between CO and CO<sub>2</sub>, with the later transects likely affected by nearby CO or CO<sub>2</sub> emissions. Due to the strong interference from HGB urban emissions, no clear correlation between CO and CO<sub>2</sub> could be found in the Parish plume.

Concentrations of SO<sub>2</sub> and reactive nitrogen species in PPPs are strongly affected by chemical reactions, heterogeneous conversion, deposition, dispersion, and cloud processing. Dispersion is expected to have the same extent of impact on both conservative (e.g., CO<sub>2</sub> and CO) and non-conservative species (e.g., SO<sub>2</sub>, NO<sub>x</sub>, HNO<sub>3</sub>, and PAN). Thus, the variations of slopes between non-conservative and conservative species reflect the impact of plume chemistry, deposition and heterogeneous processing on non-conservative species.

Given that SO<sub>2</sub> and CO<sub>2</sub> were observed to be strongly correlated in all plumes, CO<sub>2</sub> could serve well as a signature of PPPs. However, since CO<sub>2</sub> is not modeled by CMAQ, CO is selected as the conservative species for model-observation comparisons. CO is a signature emission of some but not all power plants in Texas. In observed PPPs, only in the Martin Lake and Monticello plumes could the strong correlations between the non-conservative species and CO be found at all transects. In Big Brown and Welsh plumes, SO<sub>2</sub> strongly correlates with CO, only in the initial transects.

#### **4.3 Evaluation of SO<sub>2</sub> plume evolution**

MODIS images ([http://ladsweb.nascom.nasa.gov/browse\\_images/](http://ladsweb.nascom.nasa.gov/browse_images/)) and aircraft-observed photolysis rates indicate scattered cloudiness over eastern Texas on 16 September and clear skies on 19 and 25 September (Figs. S8 and S9). Relative humidity reached saturation between 1800~1000 m during descents through the Martin Lake plume on 16 September, implying clouds distributed at that altitude and potentially interacting with the plume (Ma-4 and Ma-5 in Fig. S1). The model successfully simulated the MODIS-observed distribution of scattered clouds over northeastern Texas on that day (Fig. S9 and S10), but placed them predominately between 2500

1 and 4000 m altitude (Fig. S10), well above the plumes (Fig. S11 and S12). Thus, no significant  
2 cloud processing was modeled to occur in the base modeling.

3 Under the clear skies of 19 September (Fig.S9), the normalized SO<sub>2</sub> to CO ratio from the  
4 model and the normalized SO<sub>2</sub> to CO<sub>2</sub> ratio from the observation matched closely for the Parish  
5 plume, showing slow SO<sub>2</sub> loss (Fig. 8). At the plume age of 11 hours, only 25% SO<sub>2</sub> was  
6 removed in both the modeling and the observation. SO<sub>2</sub> loss was also slow in the Big Brown and  
7 Parish plumes during cloud-free days (Fig. 5 and 8). Thus, the model can capture SO<sub>2</sub> evolution  
8 when no cloud processing occurs.

9 However, plume observations demonstrate rapid loss of SO<sub>2</sub> in the 16 September plumes  
10 (Martin Lake, Monticello and Welsh) where scattered clouding was observed (Fig. 5). For the  
11 Martin Lake transects, the decreasing trend of SO<sub>2</sub>/CO fits to an exponential function with a  
12 first-order loss rate of 0.38 hour<sup>-1</sup>, the inverse of which is a lifetime of 2.6 hours ( $R^2=0.94$ ) (Fig.  
13 5). SO<sub>2</sub>/CO from the model decreases far slower as plume ages with a loss rate of 0.016 hour<sup>-1</sup>  
14 (lifetime of 62.5 hours), which suggests the model significantly underestimates SO<sub>2</sub> loss for the  
15 Martin Lake plume. Similarly, for the Monticello plume, the curve fit of observed SO<sub>2</sub>/CO  
16 indicates an SO<sub>2</sub> lifetime of 2.7 hours compared to a modeled SO<sub>2</sub> lifetime of 17.2 hours.  
17 Although SO<sub>2</sub> and CO were not strongly correlated in observations of the other plumes,  
18 diminishing SO<sub>2</sub>/CO<sub>2</sub> ratios indicate that rapid SO<sub>2</sub> loss also occurred in the Welsh plume.

19 The lifetime of SO<sub>2</sub> against gas-phase oxidation by OH is a few days to one week, and SO<sub>2</sub>  
20 lifetime against dry deposition approximates one day in the boundary layer. Thus, gas-phase  
21 oxidation and dry deposition are insufficient to explain the rapid loss of SO<sub>2</sub> in the 16 September  
22 plumes.

1        Could CMAQ have simulated the rapid SO<sub>2</sub> loss on 16 September if the meteorological  
2        model had placed the clouds at lower altitudes in contact with the PPPs? The cloud module in  
3        CMAQ includes two mechanisms for removing pollutants: aqueous chemical reactions and  
4        scavenging and wet deposition. SO<sub>2</sub> absorption into cloud droplets and subsequent oxidation are  
5        explicitly represented. The absorption is governed by thermodynamic equilibrium, followed by  
6        oxidation of aqueous S(IV) to S(VI) by H<sub>2</sub>O<sub>2</sub>, O<sub>3</sub>, metal ions (Fe(III) and Mn(II)), and  
7        methylhydroperoxide (MHP), and peroxyacetic acid (PAA). Since no precipitation was observed  
8        or modeled during the airborne measurements, pollutants were not expected to be scavenged.

9        Cloud parameters of meteorological inputs are perturbed to diagnose how efficiently  
10       pollutants such as SO<sub>2</sub> and NO<sub>y</sub> would have been removed from plumes. Specifically, the cloud  
11       bottom height in the meteorological field on 16 September is adjusted to 1000 meters so that the  
12       plumes interact with clouds during their transport. Liquid water content (QC) is the cloud  
13       parameter determining the extent of the pollutant aqueous processing must be larger than 0.01  
14       g/kg to trigger the cloud aqueous module. In the perturbation cases, we uniformly increase QC to  
15       0.05 g/kg ( $\approx 0.05 \text{ g/m}^3$ , equivalent to fog), 0.5 g/kg ( $\approx 0.5 \text{ g/m}^3$ , equivalent to stratocumulus  
16       clouds), and 5 g/kg ( $\approx 5 \text{ g/m}^3$ , equivalent to cumulonimbus clouds).

17       In the base modeling for the Martin Lake plume, only 11% SO<sub>2</sub> is removed in the model (the  
18       normalized SO<sub>2</sub>/CO decreased to 0.89 from Ma-1 to Ma-12). In the QC\_0.05 case, 25% of SO<sub>2</sub> is  
19       removed during that span, far short of the observed 92% SO<sub>2</sub> removal (Fig. 5). The cloudier  
20       scenarios yield 66% (QC=0.5 g/kg) and 81% (QC=5.0 g/kg) SO<sub>2</sub> removal, still below the  
21       observed rate.

22       Five S(IV) oxidation reactions are explicitly implemented in the cloud aqueous module, i.e.  
23       H<sub>2</sub>O<sub>2</sub>, O<sub>3</sub>, metal (Fe(III) and Mn(II)), MHP, and PAA oxidations. In QC\_0.05, S(IV) oxidation

1 is dominated by  $\text{H}_2\text{O}_2$  oxidation, with 96.2% of S(IV) oxidation occurring by  $\text{H}_2\text{O}_2$  in the Martin  
2 Lake plume. Only about 1.7% of S(IV) oxidation was by the metal ions.

3 In the default CMAQ cloud module, Fe(III) and Mn(II) are uniformly set to 0.01 and 0.005  
4  $\mu\text{g}/\text{m}^3$ , representative of the background atmosphere. However, power plants are major emission  
5 sources of particulate metals (Alexander et al., 2009), and may have much higher levels of  
6 Fe(III) and Mn(II), thus potentially enhancing the aqueous oxidation of sulfur in PPPs. In  
7 another perturbation case, both Fe(III) and Mn(II) concentrations are increased by a factor of 10  
8 in the QC\_0.05 case (called QC\_METAL hereafter). The increase of Fe(III) and Mn(II) is  
9 within the range of metal ion concentrations measured in fogs and cloud water (Raja et al.,  
10 2005;Parazols et al., 2006).  $\text{SO}_2$  removal in QC\_METAL was more rapid than that of QC\_0.05  
11 (Fig. 5). At the last plume transect,  $\text{SO}_2$  decreased by 33%, compared to the 25%  $\text{SO}_2$  removal in  
12 QC\_0.05, suggesting the increased metals in plume lead to more rapid  $\text{SO}_2$  oxidation. Thus,  
13 some combination of enhancements in cloud liquid water content and metals concentrations may  
14 help explain the observed rapid  $\text{SO}_2$  loss rates in the cloudy day plumes.

15 Few studies have observed rapid  $\text{SO}_2$  loss in anthropogenic plumes, though similar rates of  
16  $\text{SO}_2$  loss have been found in volcanic plumes (Oppenheimer et al., 2010;Rodríguez et al., 2008).  
17 These studies proposed that cloud aqueous processing is the mechanism for the rapid  $\text{SO}_2$   
18 removal. The comprehensive airborne measurement of plume concentrations and meteorological  
19 parameters supported by satellite images in this study confirms that the cloud processing caused  
20 the rapid  $\text{SO}_2$  loss.  $\text{SO}_2$  uptake by cloud droplet and subsequent aqueous oxidation are a major  
21 challenge to models. Earlier studies have also found that models can underestimate  $\text{SO}_2$  loss  
22 rates in clouds (Crutzen and Lawrence, 2000;Kreidenweis et al., 1997).

#### 4.4 Evaluation of plume chemistry of reactive nitrogen

In PPPs,  $\text{HNO}_3$ ,  $\text{NO}_3$ ,  $\text{N}_2\text{O}_5$ , PAN, and other organic nitrates are formed via  $\text{NO}_x$  chemical reactions. Freshly emitted  $\text{NO}_x$  titrates  $\text{O}_3$  and consumes OH, resulting in slow formation of  $\text{HNO}_3$  and no formation of PAN in the initial plume (Karamchandani et al., 1998). As a plume dilutes, OH levels recover and  $\text{HNO}_3$  and other products form from  $\text{NO}_x$  oxidation. Previous daytime observations of PPPs concluded that  $\text{HNO}_3$  and PAN were the major (more than 90%) products of  $\text{NO}_x$  oxidation in PPPs (Neuman et al., 2006; Neuman et al., 2004; Ryerson et al., 2003; Ryerson et al., 2001). The observational data in this study also show that  $\text{HNO}_3$  and PAN were the only two major oxidation products in PPPs, with  $\text{NO}_3$  and  $\text{N}_2\text{O}_5$  and other organic nitrates at least one order of magnitude lower in plume transects.

The measured and modeled  $\text{NO}_x$ ,  $\text{HNO}_3$ , and PAN are shown for comparison in Fig. S2 and S3.  $\text{NO}_x$  was higher than  $\text{HNO}_3$  until the plume transported 2.0 hours at Ma-7 and Ma-8. The model generally captured the observed evolution of reactive nitrogen species  $\text{NO}_x$ ,  $\text{HNO}_3$ , and PAN in the plume, simulating the transition from  $\text{NO}_x$  to  $\text{HNO}_3$  dominance and approximately matching the observed PAN levels. However, the simulated  $\text{HNO}_3$  concentrations were higher than observed, implying over-prediction of  $\text{HNO}_3$  formation or under-prediction of  $\text{HNO}_3$  loss.

The oxidation of  $\text{NO}_x$  by radicals approximates as a first-order reaction if radical concentrations are assumed to be constant in the plume. The observed  $\text{NO}_x/\text{CO}$  fits to an exponential decay function (for Martin Lake,  $R^2=0.85$ ; for Monticello,  $R^2=0.86$ ; Fig. 6), corresponding to  $\text{NO}_x$  lifetimes of 2.6 and 1.2 hours for the Martin Lake and Monticello plumes, respectively. The  $\text{NO}_x$  lifetimes computed here are consistent with the  $\text{NO}_x$  lifetimes (1.0~1.6 hours) estimated for both plants in TexAQS 2000 (Neuman et al., 2004). The declining trends of  $\text{NO}_x/\text{CO}$  from the model and the observation closely match in the Martin Lake and Monticello

1 plumes, with discrepancies only in the initial transects due to the inability of the model to resolve  
2 subgrid-scale plume structure (Fig. 6).

3 The ratios of  $\text{HNO}_3/\text{CO}$  and  $\text{PAN}/\text{CO}$  are compared between the model and observations to  
4 explore chemical evolution in the Martin Lake and Monticello plumes. We find that the model  
5 captures the PAN formation very well, closely matching observed trends as the plumes age (Fig.  
6 6 and Fig. S2). The modeled  $\text{HNO}_3/\text{CO}$ , however, was 0.7~6.6 times larger than observed. Given  
7 the good agreement between the modeled and observed  $\text{NO}_x$  oxidation and PAN formation, the  
8  $\text{HNO}_3$  gap between the model and the observation on the cloudy day implies that  $\text{HNO}_3$ , while  
9 formed during plume transport, was rapidly removed from the atmosphere, which is not captured  
10 by the model.

11 Unexpectedly rapid loss of  $\text{NO}_y$  has also been reported by some measurement studies of  
12 biomass burning (Takegawa et al., 2003) and PPPs (Neuman et al., 2004), but not in others  
13 (Ryerson et al., 2003). When  $\text{NO}_x$  is oxidized to other reactive nitrogen species, the reactive  
14 nitrogen may be removed from the atmosphere via rain scavenging, dry deposition,  
15 heterogeneous conversion to aerosol, and cloud processing, resulting in the loss of  $\text{NO}_y$ .  
16 Assuming a first-order decline of  $\text{NO}_y/\text{CO}$  (Fig. 7), the observed  $\text{NO}_y$  loss rate was  $0.15 \text{ hour}^{-1}$   
17 for the Martin Lake plume whereas the modeled  $\text{NO}_y$  loss rate was lower by a factor of 6 ( $0.026$   
18  $\text{hour}^{-1}$ ). For the Monticello plume, the observed  $\text{NO}_y$  loss rate ( $0.24 \text{ hour}^{-1}$ ) was 2.3 times the  
19 modeled. The observed  $\text{NO}_y/\text{CO}_2$  in Martin Lake, Monticello, and Welsh plumes had a similar  
20 extent of  $\text{NO}_y$  loss, especially during the early plume age ( $\leq 2$  hours) when  $\text{NO}_y/\text{CO}$  declined by  
21 40~50% (Fig. 7).

22 On 19 September, a cloud-free day, the model effectively simulates the observed slow  
23 removal of  $\text{NO}_y$  (Fig 8).  $\text{NO}_y$  loss on the cloudy day likely reflects deposition of highly soluble

1 HNO<sub>3</sub>, since the other main NO<sub>y</sub> constituents (NO<sub>x</sub> and PAN) have low water solubility, cannot  
2 directly convert to aerosol, and have negligible dry deposition in plume. NO<sub>x</sub> oxidation and  
3 thermal decomposition of PAN do not shift the gas-phase NO<sub>y</sub> budget since their products are  
4 also gas-phase NO<sub>y</sub> constituents. The measured NO<sub>3</sub><sup>-</sup> was minor in the inorganic aerosol  
5 composition, indicating that the loss of HNO<sub>3</sub> to aerosol-NO<sub>3</sub><sup>-</sup> was negligible under the high  
6 ambient temperatures (the measured average temperature was 28.9°C) and the lack of ammonia  
7 enhancement beyond levels needed to neutralize the sulfate in the PPPs (Nowak et al., 2010).  
8 Given that no wet precipitation was reported on the flight days, no rain scavenging is expected to  
9 have occurred. HNO<sub>3</sub> may have rapidly dissolved in cloud droplets if the plume interacted with a  
10 cloud, as is possible under the 16 September scattered cloudiness conditions discussed earlier.

11 In contrast to the SO<sub>2</sub> results, the cloud perturbation scenarios did not significantly impact  
12 modeled concentrations of NO<sub>y</sub> species. Among NO<sub>y</sub> species, HNO<sub>3</sub> is the only one to be  
13 processed by the cloud module. Even raising QC to 5.0 g/kg, there is no scavenging removal of  
14 HNO<sub>3</sub> since no wet deposition happens in the absence of precipitation. At the end of the cloud  
15 module, CMAQ returns the aqueous concentration of HNO<sub>3</sub> in cloud to either gas-phase or  
16 aerosol species, keeping the ratio of HNO<sub>3</sub> to total NO<sub>y</sub> constant. This makes HNO<sub>3</sub>  
17 concentrations insensitive to QC in CMAQ.

#### 18 **4.5 Evaluation of O<sub>3</sub> simulation in PPPs**

19 Various numerical models have been applied to simulate the O<sub>3</sub> chemistry of PPPs (Sillman,  
20 2000;Springston et al., 2005;Frost et al., 2006;Zaveri et al., 2010). The simulation of the  
21 chemistry and transport of PPPs by 3-D models are widely used for assessing the effectiveness of  
22 emission controls of power plant pollutants. However, the performance of these models has most

often been evaluated with ground concentrations (Mauzerall et al., 2005; Vijayaraghavan et al., 2009; Godowitch et al., 2008a; Godowitch et al., 2008b).

The model overestimated background  $O_3$  by 8~15 ppb during the flights (Table S4). Sensitivity modeling shows that boundary conditions were the biggest contributor to background  $O_3$  levels. Thus, we focus on the differences ( $\Delta O_3$ ) between plume and background  $O_3$  mixing ratios to assess model performance for  $O_3$  formation from power plant plumes (Table S4).

The model accurately simulates that the Monticello and Welsh plumes shift from being depleted to being enriched in  $O_3$  between transect 1 and 2, and predicts the transition to occur one transect sooner than observed for Martin Lake. All of these plumes traversed rural regions of northeastern Texas where biogenic isoprene is abundant. However, the model underestimates the amount of  $O_3$  enrichment downwind by 20-70% (Ma-9 to Ma-12, Mo-2 to Mo-4, We-2 to We-4). The model also underestimates titration in the initial transects, reflecting the more rapid dilution of  $NO_x$  in the model.

Ozone Production Efficiency (OPE) quantifies the number of  $O_3$  molecules formed per molecule of  $NO_x$  irreversibly oxidized to  $NO_z$  species (Liu et al., 1987). Here, we determine OPE in the model from the ratio  $ZOC_{O_3}$  to  $ZOC_{NO_z}$ , and in the measurements from the least square slope of  $O_3$  versus  $NO_y-NO_x$  ( $NO_z$ ) (Trainer et al., 1993; Kleinman et al., 2002; Griffin et al., 2004; Ryerson et al., 2003).

Observations of Martin Lake, Monticello, and Welsh transects show OPE steadily increasing, while  $O_3$  production evolves from depletion to net formation, consistent with OPE trends from PPPs in the southeast U.S. (Ryerson et al., 2001) and in Texas in 2000 (Springston et al., 2005; Ryerson et al., 2003). OPEs from transects of these plumes (Ma-6, Mo-4, and We-4) at similar plume ages are compared in Fig. 9. OPEs for Monticello and Welsh were remarkably

1 similar (Fig. 9), reflecting approximately equal O<sub>3</sub> formation potentials of these facilities with  
2 similar NO<sub>x</sub> emission rates (Table 1). Martin Lake emitted about two times as much NO<sub>x</sub> as  
3 Monticello and Welsh, and thus exhibited a smaller OPE. Comparing younger transects, OPE in  
4 the Big Brown plume (Bi-1) was 1.7 at a plume age of 1.3 hours, lower than the similar-plume-  
5 age OPE of Martin Lake (2.6, Ma-3) and Welsh (4.6, We-2), but close to the OPE of Monticello  
6 (1.4, Mo-2). OPE could not be quantified in the subsequent Big Brown transect due to lack of  
7 correlation between O<sub>3</sub> and NO<sub>z</sub>. The Parish plume exhibited an OPE of 4.4 at a plume age of  
8 just 0.6 hours, suggesting rapid O<sub>3</sub> formation under the influence of Houston region  
9 anthropogenic VOCs.

10 The model replicated the observed temporal trends in OPE but simulated maximum OPEs  
11 about a factor of 2 lower than observed (Table S4). Since the calculation of OPE implicitly  
12 assumes that NO<sub>y</sub> is conservative in plumes, the rapid loss of NO<sub>y</sub> observed but not modeled on  
13 the cloudy day (Table S4) may undermine the accuracy of the observation-based OPE.

14 It should also be noted that the model tended to under-predict measured isoprene  
15 concentrations. Observed isoprene concentrations averaged over all transects are higher than the  
16 modeled average by 51.3%. We perturb domain-wide isoprene emission rates by this factor in  
17 the model to investigate how much impact the isoprene discrepancy has on the O<sub>3</sub> formation in  
18 plumes. After perturbation, the simulated ZOC<sub>O3</sub> has a maximum increase of 3 ppb (Ma-2). The  
19 maximum O<sub>3</sub> increase for Monticello and Welsh is 1.5 and 2 ppb, respectively. OPEs of Martin  
20 Lake, Monticello, and Welsh plumes would increase to 7.0, 7.8, and 5.9, respectively, closing  
21 roughly half of the gap between modeled and observed OPEs. For Big Brown, the OPE would  
22 increase by a factor of 1.4, and for Parish, the OPE would increase to 6 (Pa-2), exceeding the  
23 observed OPE (4.4).

## 5 Summary and Conclusions

A regional 3D photochemical model was applied with fine-grid resolution to simulate PPPs during three days of airborne measurement by NOAA's WP-3 aircraft in TexAQS II. In this modeling study, the modeled and airborne observed concentrations are compared in detail at each plume transect. Under steady wind meteorological conditions, the fine-scale (4km) CMAQ accurately simulated the transport and dispersion of PPPs despite lacking a plume-in-grid module.

SO<sub>2</sub> and NO<sub>x</sub> show strong consistencies among the CEMS-reported emission data. In the Martin Lake and Monticello plumes, CO was strongly correlated with SO<sub>2</sub> and NO<sub>y</sub> and could serve as a conservative tracer species to track plume evolution; CO<sub>2</sub> was strongly correlated with SO<sub>2</sub> and NO<sub>y</sub> in all plumes but was not modeled by CMAQ. The trend in the least square slopes of pollutants relative to CO (CO<sub>2</sub>) was used to assess species lifetime.

On clear-sky days (19 and 25 September), SO<sub>2</sub> and NO<sub>y</sub> experienced slow evolution (loss) in the Parish and Big Brown plumes. Both the model and the observation were closely correlated in the ratios of SO<sub>2</sub> and NO<sub>y</sub> to conservative species, suggesting the model well captured SO<sub>2</sub> and NO<sub>y</sub> evolution in the plumes.

SO<sub>2</sub> was observed to be rapidly lost in the Martin Lake, Monticello, and Welsh plumes under scattered cloudiness on 16 September. The observation-based SO<sub>2</sub> lifetime was 2.6 and 2.7 hours for the Martin Lake and Monticello plumes, respectively. The detailed examination of the photolysis rate and relative humidity data suggested cloud-processing of PPPs caused the rapid SO<sub>2</sub> loss on 16 September. The original simulation did not show the apparent SO<sub>2</sub> loss since

1 PPPs resided below clouds in the model. Perturbing the cloud bottom heights to interact with the  
2 PPPs yielded modest rates of SO<sub>2</sub> removal via aqueous processing in the CMAQ cloud module.  
3 SO<sub>2</sub> removal in the model was still slower than the observed rapid loss, even after increasing  
4 cloud liquid water content and metals concentrations in cloud droplets to enhance SO<sub>2</sub> oxidation.

5 The simulation closely matched the observed NO<sub>x</sub> oxidation rates. The observed NO<sub>x</sub>  
6 lifetime for Martin Lake and Monticello plumes was 2.6 hours and 1.2 hours, respectively. The  
7 modeled PAN formation reflected the observed trend of PAN formation, while the modeled  
8 HNO<sub>3</sub> was 0.7~6.6 times higher than observed due to the rapid HNO<sub>3</sub> loss in observation on  
9 cloudy days. For the Martin Lake plume, the loss rate of NO<sub>y</sub> has been quantified to be 0.148  
10 hour<sup>-1</sup> in observation, faster than the modeled NO<sub>y</sub> (0.026 hour<sup>-1</sup>) by a factor of 6 since modeled  
11 NO<sub>y</sub> loss was insensitive to aqueous processing in the absence of precipitation.

12 The model effectively simulated the transition between ozone titration and formation but  
13 tended to predict lower OPE than indicated by observations. The discrepancies of OPEs between  
14 the model and the observations could be explained by the observed rapid NO<sub>y</sub> loss that biases  
15 high the observation-based OPE estimates.

## 17 **Acknowledgments**

18 The work of W. Zhou and D. S. Cohan was funded by the Shell Center for Sustainability at  
19 Rice University and National Science Foundation CAREER Award Grant 087386. We thank  
20 Robert Griffin at Rice University for helpful discussions on data analyses. We thank Ken Aikin  
21 and Harald Stark in the NOAA ESRL Chemical Sciences Division for help in using

meteorological and photolysis data. Although this article has been reviewed by the US EPA and approved for publication, it does not necessarily reflect EPA policies or views.

## References

- Akimoto, H.: Global Air Quality and Pollution, *Science*, 302, 1716-1719, 10.1126/science.1092666, 2003.
- Alexander, B., Park, R. J., Jacob, D. J., and Gong, S.: Transition metal-catalyzed oxidation of atmospheric sulfur: Global implications for the sulfur budget, *J. Geophys. Res.*, 114, D02309, 10.1029/2008jd010486, 2009.
- Appel, K. W., Roselle, S. J., Gilliam, R. C., and Pleim, J. E.: Sensitivity of the Community Multiscale Air Quality (CMAQ) Model v4.7 results for the eastern United States to MM5 and WRF meteorological drivers, *Geosci. Model Dev. Discuss.*, 2, 1081-1114, 2009.
- Brock, C. A., Washenfelder, R. A., Trainer, M., Ryerson, T. B., Wilson, J. C., Reeves, J. M., Huey, L. G., Holloway, J. S., Parrish, D. D., Hübler, G., and Fehsenfeld, F. C.: Particle growth in the plumes of coal-fired power plants, *J. Geophys. Res. - Atmos.*, 107, 10.1029/2001jd001062, 2002.
- Brock, C. A., Trainer, M., Ryerson, T. B., Neuman, J. A., Parrish, D. D., Holloway, J. S., Nicks, D. K., Jr., Frost, G. J., Hübler, G., Fehsenfeld, F. C., Wilson, J. C., Reeves, J. M., Lafleur, B. G., Hilbert, H., Atlas, E. L., Donnelly, S. G., Schauffler, S. M., Stroud, V. R., and Wiedinmyer, C.: Particle growth in urban and industrial plumes in Texas, *J. Geophys. Res. - Atmos.*, 108, 10.1029/2002jd002746, 2003.
- Brown, S. S., Dubé, W. P., Fuchs, H., Ryerson, T. B., Wollny, A. G., Brock, C. A., Bahreini, R., Middlebrook, A. M., Neuman, J. A., Atlas, E., Roberts, J. M., Osthoff, H. D., Trainer, M., Fehsenfeld, F. C., and Ravishankara, A. R.: Reactive uptake coefficients for N<sub>2</sub>O<sub>5</sub> determined from aircraft measurements during the Second Texas Air Quality Study: Comparison to current model parameterizations, *J. Geophys. Res. - Atmos.*, 114, D00F10, 10.1029/2008jd011679, 2009.
- Byun, D., and Schere, K. L.: Review of the Governing Equations, Computational Algorithms, and Other Components of the Models-3 Community Multiscale Air Quality (CMAQ) Modeling System, *Appl. Mech. Rev.*, 59, 27-50, 2006.
- Colella, P., and Woodward, P. R.: The Piecewise Parabolic Method (PPM) for gas-dynamical simulations, *Journal of Computational Physics*, 54, 174-201, 1984.
- Crutzen, P. J., and Lawrence, M. G.: The Impact of Precipitation Scavenging on the Transport of Trace Gases: A 3-Dimensional Model Sensitivity Study, *Journal of Atmospheric Chemistry*, 37, 81-112, 10.1023/a:1006322926426, 2000.
- Dudhia, J.: Numerical study of convection observed during the winter monsoon experiment using a mesoscale two-dimensional model, *J. Atmos. Sci.*, 46, 3077-3107, 1989.

1 EPA: Sparse Matrix Operational Kernel Emission model version 2.4 User's Manual,  
2 <http://www.smoke-model.org/version2/index.cfg>, (last access: October 2009), 2006., 2006.

3 EPA, U. S.: NOx Budget Trading Program 2003 progress and compliance report, Rep. EPA-430-  
4 R-04-010, Clean Air Markets Div., Off. of Air and Radiat., Washington, D. C. , 2004.

5 EPA, U. S.: Acid Rain Program 2002 progress report, Rep. EPA-430-R-03-011, Clean Air  
6 Markets Div., Off. of Air and Radiat., Washington, D. C. , 2005.

7 Flues, M., Hama, P., Lemes, M. J. L., Dantas, E. S. K., and Fornaro, A.: Evaluation of the  
8 rainwater acidity of a rural region due to a coal-fired power plant in Brazil, *Atmos. Environ.*, 36,  
9 2397-2404, 2002.

10 Foley, K. M., Roselle, S. J., Appel, K. W., Bhawe, P. V., Pleim, J. E., Otte, T. L., Mathur, R.,  
11 Sarwar, G., Young, J. O., Gilliam, R. C., Nolte, C. G., Kelly, J. T., Gilliland, A. B., and Bash, J.  
12 O.: Incremental testing of the Community Multiscale Air Quality (CMAQ) modeling system  
13 version 4.7, *Geosci. Model Dev.*, 3, 205-226, 10.5194/gmd-3-205-2010, 2010.

14 Frost, G. J., McKeen, S. A., Trainer, M., Ryerson, T. B., Neuman, J. A., Roberts, J. M.,  
15 Swanson, A., Holloway, J. S., Sueper, D. T., Fortin, T., Parrish, D. D., Fehsenfeld, F. C., Flocke,  
16 F., Peckham, S. E., Grell, G. A., Kowal, D., Cartwright, J., Auerbach, N., and Habermann, T.:  
17 Effects of changing power plant NOx emissions on ozone in the eastern United States: Proof of  
18 concept, *J. Geophys. Res. - Atmos.*, 111, 10.1029/2005jd006354, 2006.

19 Godowitch, J. M., Gilliland, A. B., Draxler, R. R., and Rao, S. T.: Modeling assessment of point  
20 source NOx emission reductions on ozone air quality in the eastern United States, *Atmos.*  
21 *Environ.*, 42, 87-100, 2008a.

22 Godowitch, Hogrefe, C., and Rao, S. T.: Diagnostic analyses of a regional air quality model:  
23 Changes in modeled processes affecting ozone and chemical-transport indicators from NOx  
24 point source emission reductions, *J. Geophys. Res. - Atmos.*, 113, 10.1029/2007jd009537,  
25 2008b.

26 Grell, G. A., Dudhia, J., and Stauffer, D. R.: A description of the Fifth-Generation Penn  
27 State/NCAR Mesoscale Model (MM5). NCAR Technical Note NCAR/TN-398+STR, 1994.

28 Griffin, R. J., Johnson, C. A., Talbot, R. W., Mao, H., Russo, R. S., Zhou, Y., and Sive, B. C.:  
29 Quantification of ozone formation metrics at Thompson Farm during the New England Air  
30 Quality Study (NEAQS) 2002, *J. Geophys. Res. - Atmos.*, 109, D24302, 10.1029/2004jd005344,  
31 2004.

32 Kain, J. S.: The Kain-Fritsch convective parameterization: An update, *J. Appl. Meteorol.*, 43,  
33 170-181, 2004.

34 Karamchandani, P., Koo, A., and Seigneur, C.: Reduced Gas-Phase Kinetic Mechanism for  
35 Atmospheric Plume Chemistry, *Environ. Sci. Technol.*, 32, 1709-1720, 10.1021/es970707u,  
36 1998.

37 Kim, S. W., Heckel, A., McKeen, S. A., Frost, G. J., Hsie, E. Y., Trainer, M. K., Richter, A.,  
38 Burrows, J. P., Peckham, S. E., and Grell, G. A.: Satellite-observed U.S. power plant NOx  
39 emission reductions and their impact on air quality, *Geophys. Res. Lett.*, 33,  
40 10.1029/2006gl027749, 2006.

1 Kleinman, L. I., Daum, P. H., Lee, Y.-N., Nunnermacker, L. J., Springston, S. R., Weinstein-  
2 Lloyd, J., and Rudolph, J.: Ozone production efficiency in an urban area, *J. Geophys. Res. -*  
3 *Atmos.*, 107, 4733, 10.1029/2002jd002529, 2002.

4 Kreidenweis, S. M., Zhang, Y., and Taylor, G. R.: The effects of clouds on aerosol and chemical  
5 species production and distribution 2. Chemistry model description and sensitivity analysis, *J.*  
6 *Geophys. Res.*, 102, 23867-23882, 10.1029/97jd00775, 1997.

7 Liu, S. C., Trainer, M., Fehsenfeld, F. C., Parrish, D. D., Williams, E. J., Fahey, D. W., Hübler,  
8 G., and Murphy, P. C.: Ozone Production in the Rural Troposphere and the Implications for  
9 Regional and Global Ozone Distributions, *J. Geophys. Res. - Atmos.*, 92, 4191-4207,  
10 10.1029/JD092iD04p04191, 1987.

11 Mauzerall, D. L., Sultan, B., Kim, N., and Bradford, D. F.: NO<sub>x</sub> emissions from large point  
12 sources: variability in ozone production, resulting health damages and economic costs, *Atmos.*  
13 *Environ.*, 39, 2851-2866, 2005.

14 Mlawer, E. J., Taubman, S. J., Brown, P. D., Iacono, M. J., and Clough, S. A.: Radiative transfer  
15 for inhomogeneous atmospheres: RRTM, a validated correlated-k model for the longwave, *J.*  
16 *Geophys. Res. - Atmos.*, 102, 16663-16682, 1997.

17 Neuman, J. A., Parrish, D. D., Ryerson, T. B., Brock, C. A., Wiedinmyer, C., Frost, G. J.,  
18 Holloway, J. S., and Fehsenfeld, F. C.: Nitric acid loss rates measured in power plant plumes, *J.*  
19 *Geophys. Res. - Atmos.*, 109, 10.1029/2004jd005092, 2004.

20 Neuman, J. A., Parrish, D. D., Trainer, M., Ryerson, T. B., Holloway, J. S., Nowak, J. B.,  
21 Swanson, A., Flocke, F., Roberts, J. M., Brown, S. S., Stark, H., Sommariva, R., Stohl, A.,  
22 Peltier, R., Weber, R., Wollny, A. G., Sueper, D. T., Hubler, G., and Fehsenfeld, F. C.: Reactive  
23 nitrogen transport and photochemistry in urban plumes over the North Atlantic Ocean, *J.*  
24 *Geophys. Res. - Atmos.*, 111, 10.1029/2005jd007010, 2006.

25 Neuman, J. A., Nowak, J. B., Zheng, W., Flocke, F., Ryerson, T. B., Trainer, M., Holloway, J.  
26 S., Parrish, D. D., Frost, G. J., Peischl, J., Atlas, E. L., Bahreini, R., Wollny, A. G., and  
27 Fehsenfeld, F. C.: Relationship between photochemical ozone production and NO<sub>x</sub> oxidation in  
28 Houston, Texas, *J. Geophys. Res. - Atmos.*, 114, 10.1029/2008jd011688, 2009.

29 Nicks, D. K., Holloway, J. S., Ryerson, T. B., Dissly, R. W., Parrish, D. D., Frost, G. J., Trainer,  
30 M., Donnelly, S. G., Schauffler, S., Atlas, E. L., Hubler, G., Sueper, D. T., and Fehsenfeld, F. C.:  
31 Fossil-fueled power plants as a source of atmospheric carbon monoxide, *J. Environ. Monitor.*, 5,  
32 35-39, 2003.

33 Nowak, J. B., Neuman, J. A., Bahreini, R., Brock, C. A., Middlebrook, A. M., Wollny, A. G.,  
34 Holloway, J. S., Peischl, J., Ryerson, T. B., and Fehsenfeld, F. C.: Airborne observations of  
35 ammonia and ammonium nitrate formation over Houston, Texas, *J. Geophys. Res. - Atmos.*, In  
36 press, 2010.

37 Nunnermacker, L. J., Kleinman, L. I., Imre, D., Daum, P. H., Lee, Y. N., Lee, J. H., Springston,  
38 S. R., Newman, L., and Gillani, N.: NO<sub>y</sub> lifetimes and O<sub>3</sub> production efficiencies in urban and  
39 power plant plumes: Analysis of field data, *J. Geophys. Res. - Atmos.*, 105, 9165-9176,  
40 10.1029/1999jd900753, 2000.

1 Oppenheimer, C., Kyle, P., Eisele, F., Crawford, J., Huey, G., Tanner, D., Kim, S., Mauldin, L.,  
2 Blake, D., Beyersdorf, A., Buhr, M., and Davis, D.: Atmospheric chemistry of an Antarctic  
3 volcanic plume, *J. Geophys. Res. - Atmos.*, 115, D04303, 10.1029/2009jd011910, 2010.

4 Otte, T. L., and Pleim, J. E.: The Meteorology-Chemistry Interface Processor (MCIP) for the  
5 CMAQ modeling system, *Geosci. Model Dev. Discuss.*, 2, 1449-1486, 2009.

6 Parazols, M., Marinoni, A., Amato, P., Abida, O., Laj, P., and Mailhot, G.: Speciation and role of  
7 iron in cloud droplets at the puy de Dôme station, *Journal of Atmospheric Chemistry*, 54, 267-  
8 281, 10.1007/s10874-006-9026-x, 2006.

9 Parrish, D. D., Allen, D. T., Bates, T. S., Estes, M., Fehsenfeld, F. C., Feingold, G., Ferrare, R.,  
10 Hardesty, R. M., Meagher, J. F., Nielsen-Gammon, J. W., Pierce, R. B., Ryerson, T. B., Seinfeld,  
11 J. H., and Williams, E. J.: Overview of the Second Texas Air Quality Study (TexAQS II) and the  
12 Gulf of Mexico Atmospheric Composition and Climate Study (GoMACCS), *J. Geophys. Res. -*  
13 *Atmos.*, 114, 10.1029/2009jd011842, 2009.

14 Peischl, J., Ryerson, T. B., Holloway, J. S., Parrish, D. D., Trainer, M., Frost, G. J., Aikin, K. C.,  
15 Brown, S. S., Dubé, W. P., Stark, H., and Fehsenfeld, F. C.: A top-down analysis of emissions  
16 from selected Texas power plants during TexAQS 2000 and 2006, *J. Geophys. Res. - Atmos.*,  
17 115, D16303, 10.1029/2009jd013527, 2010.

18 Pleim, J. E.: A Combined Local and Nonlocal Closure Model for the Atmospheric Boundary  
19 Layer. Part I: Model Description and Testing, *J. Appl. Meteorol. Clim.*, 46, 1383-1395,  
20 doi:10.1175/JAM2539.1, 2007.

21 Raja, S., Ravikrishna, R., Kommalapati, R., and Valsaraj, K.: Monitoring of Fogwater Chemistry  
22 in the Gulf Coast Urban Industrial Corridor: Baton Rouge (Louisiana), *Environmental*  
23 *Monitoring and Assessment*, 110, 99-120, 10.1007/s10661-005-6281-2, 2005.

24 Rodríguez, L. A., Watson, I. M., Edmonds, M., Ryan, G., Hards, V., Oppenheimer, C. M. M.,  
25 and Bluth, G. J. S.: SO<sub>2</sub> loss rates in the plume emitted by Soufrière Hills volcano, Montserrat, *J.*  
26 *Volcanol. Geoth. Res.*, 173, 135-147, 2008.

27 Ryerson, T. B., Buhr, M. P., Frost, G. J., Goldan, P. D., Holloway, J. S., Hübler, G., Jobson, B.  
28 T., Kuster, W. C., McKeen, S. A., Parrish, D. D., Roberts, J. M., Sueper, D. T., Trainer, M.,  
29 Williams, J., and Fehsenfeld, F. C.: Emissions lifetimes and ozone formation in power plant  
30 plumes, *J. Geophys. Res. - Atmos.*, 103, 10.1029/98jd01620, 1998.

31 Ryerson, T. B., Trainer, M., Holloway, J. S., Parrish, D. D., Huey, L. G., Sueper, D. T., Frost, G.  
32 J., Donnelly, S. G., Schauffler, S., Atlas, E. L., Kuster, W. C., Goldan, P. D., Hubler, G.,  
33 Meagher, J. F., and Fehsenfeld, F. C.: Observations of Ozone Formation in Power Plant Plumes  
34 and Implications for Ozone Control Strategies, *Science*, 292, 719-723, 10.1126/science.1058113,  
35 2001.

36 Ryerson, T. B., Trainer, M., Angevine, W. M., Brock, C. A., Dissly, R. W., Fehsenfeld, F. C.,  
37 Frost, G. J., Goldan, P. D., Holloway, J. S., Hübler, G., Jakoubek, R. O., Kuster, W. C., Neuman,  
38 J. A., Nicks, D. K., Jr., Parrish, D. D., Roberts, J. M., Sueper, D. T., Atlas, E. L., Donnelly, S. G.,  
39 Flocke, F., Fried, A., Potter, W. T., Schauffler, S., Stroud, V., Weinheimer, A. J., Wert, B. P.,  
40 Wiedinmyer, C., Alvarez, R. J., Banta, R. M., Darby, L. S., and Senff, C. J.: Effect of  
41 petrochemical industrial emissions of reactive alkenes and NO<sub>x</sub> on tropospheric ozone formation  
42 in Houston, Texas, *J. Geophys. Res. - Atmos.*, 108, 10.1029/2002jd003070, 2003.

1 Sillman, S.: Ozone production efficiency and loss of NO<sub>x</sub> in power plant plumes: Photochemical  
2 model and interpretation of measurements in Tennessee, *J. Geophys. Res. - Atmos.*, 105,  
3 10.1029/1999jd901014, 2000.

4 Skamarock, W. C., Klemp, J. B., Dudhia, J., Gill, D., Barker, D. M., Duda, M. G., Huang, X.-Y.,  
5 Ang, W., and Powers, J. G.: A description of the advanced research WRF version 3. NCAR  
6 Technical Note NCAR/TN 475 STR, 2008.

7 Springston, S. R., Kleinman, L. I., Brechtel, F., Lee, Y.-N., Nunnermacker, L. J., and Wang, J.:  
8 Chemical evolution of an isolated power plant plume during the TexAQS 2000 study, *Atmos.*  
9 *Environ.*, 39, 3431-3443, 2005.

10 Srivastava, R. K., Miller, C. A., Erickson, C., and Jambhekar, R.: Emissions of sulfur trioxide  
11 from coal-fired power plants, *J. Air Waste Manage. Assoc*, 54, 750-762, 2004.

12 Takegawa, N., Kondo, Y., Koike, M., Ko, M., Kita, K., Blake, D. R., Nishi, N., Hu, W., Liley, J.  
13 B., Kawakami, S., Shirai, T., Miyazaki, Y., Ikeda, H., Russel-Smith, J., and Ogawa, T.: Removal  
14 of NO<sub>x</sub> and NO<sub>y</sub> in biomass burning plumes in the boundary layer over northern Australia, *J.*  
15 *Geophys. Res. - Atmos.*, 108, 4308, 10.1029/2002jd002505, 2003.

16 Thompson, G., Rasmussen, R. M., and Manning, K.: Explicit Forecasts of Winter Precipitation  
17 Using an Improved Bulk Microphysics Scheme. Part I: Description and Sensitivity Analysis,  
18 *Mon. Weather. Rev.*, 132, 519-542, doi:10.1175/1520-0493, 2004.

19 Trainer, M., Parrish, D. D., Buhr, M. P., Norton, R. B., Fehsenfeld, F. C., Anlauf, K. G.,  
20 Bottenheim, J. W., Tang, Y. Z., Wiebe, H. A., Roberts, J. M., Tanner, R. L., Newman, L.,  
21 Bowersox, V. C., Meagher, J. F., Olszyna, K. J., Rodgers, M. O., Wang, T., Berresheim, H.,  
22 Demerjian, K. L., and Roychowdhury, U. K.: Correlation of ozone with NO<sub>y</sub> in photochemically  
23 aged air, *J. Geophys. Res. - Atmos.*, 98, 2917-2925, 10.1029/92jd01910, 1993.

24 Trainer, M., Ridley, B. A., Buhr, M. P., Kok, G., Walega, J., Hübler, G., Parrish, D. D., and  
25 Fehsenfeld, F. C.: Regional ozone and urban plumes in the southeastern United States:  
26 Birmingham, a case study, *J. Geophys. Res. - Atmos.*, 100, 18823-18834, 10.1029/95jd01641,  
27 1995.

28 Vijayaraghavan, K., Zhang, Y., Seigneur, C., Karamchandani, P., and Snell, H. E.: Export of  
29 reactive nitrogen from coal-fired power plants in the U.S.: Estimates from a plume-in-grid  
30 modeling study, *J. Geophys. Res. - Atmos.*, 114, 10.1029/2008jd010432, 2009.

31 Walcek, C. J., and Taylor, G. R.: A Theoretical Method for Computing Vertical Distributions of  
32 Acidity and Sulfate Production within Cumulus Clouds, *J. Atmos. Sci.*, 43, 339-355,  
33 doi:10.1175/1520-0469(1986)043<0339:ATMFCV>2.0.CO;2, 1986.

34 Xiu, A., and Pleim, J. E.: Development of a Land Surface Model. Part I: Application in a  
35 Mesoscale Meteorological Model, *J. Appl. Meteorol*, 40, 192-209, doi:10.1175/1520-  
36 0450(2001), 2001.

37 Yarwood, G., Rao, S., Yocke, M., and Whitten, G.: Updates to the Carbon Bond Chemical  
38 Mechanism: CB05 Final Report to the US EPA, RT-0400675, 2005.

39 Yamartino, R. J.: Nonnegative, Conserved Scalar Transport Using Grid-Cell-centered, Spectrally  
40 Constrained Blackman Cubics for Applications on a Variable-Thickness Mesh, *Monthly*

1 Weather Review, 121, 753-763, doi:10.1175/1520-0493(1993)121<0753:NCSTUG>2.0.CO;2,  
2 1993.

3 Zaveri, R. A., Berkowitz, C. M., Brechtel, F. J., Gilles, M. K., Hubbe, J. M., Jayne, J. T.,  
4 Kleinman, L. I., Laskin, A., Madronich, S., Onasch, T. B., Pekour, M. S., Springston, S. R.,  
5 Thornton, J. A., Tivanski, A. V., and Worsnop, D. R.: Nighttime chemical evolution of aerosol  
6 and trace gases in a power plant plume: Implications for secondary organic nitrate and  
7 organosulfate aerosol formation, NO<sub>3</sub> radical chemistry, and N<sub>2</sub>O<sub>5</sub> heterogeneous hydrolysis, J.  
8 Geophys. Res., 115, D12304, 10.1029/2009jd013250, 2010.

Table 1. Major power plants in eastern Texas

Facility	NO <sub>x</sub> emission rate <sup>a</sup> (tons/hour)	SO <sub>2</sub> emission rate <sup>a</sup> (tons/hour)	Stack Height (m)
Martin Lake	2.02	10.37	138
Monticello	1.34	5.49	128
Welsh	0.95	2.21	172
Pirkey	0.58	0.21	160
Big Brown	0.84	13.09	122
Parish	0.33	2.74	183
Limestone	0.79	0.63	137

<sup>a</sup> emission rate is the hourly averaged CEMS data for Martin Lake, Monticello, and Welsh on 16 September, 2006, and for Parish, Big Brown, and Limestone on 25 September, 2006.

Table 2. CEMS-reported E(SO<sub>2</sub>)/E(NO<sub>x</sub>) emission molar ratio, the observed SO<sub>2</sub>/NO<sub>y</sub> and the modeled ZOC<sub>SO2</sub>/ZOC<sub>NOy</sub> at the location of the first plume transect.

Plant	CEMS SO <sub>2</sub> /NO <sub>x</sub>	OBS SO <sub>2</sub> /NO <sub>y</sub> <sup>a</sup>	MODEL ZOC <sub>SO2</sub> /ZOC <sub>NOy</sub> <sup>b</sup>	Plume age (hours)
Martin Lake	3.05	3.94 (0.98)	3.30	0.7
Monticello	2.04	3.00 (0.86)	1.84	0.3
Welsh	1.10	1.20 (0.86)	1.08	0.4
Big Brown	8.94	10.95 (0.97)	9.73	1.3
Parish	5.28	6.83 (0.68)	5.18	0.6

<sup>a</sup> the values in brackets are the R<sup>2</sup> of least square fit of SO<sub>2</sub> versus NO<sub>y</sub>

<sup>b</sup> ZOC<sub>SO2</sub> = SO<sub>2</sub> model, base - SO<sub>2</sub> model, zero-out that plant, ZOC<sub>NOy</sub> = NO<sub>y</sub> model, base - NO<sub>y</sub> model, zero-out that plant

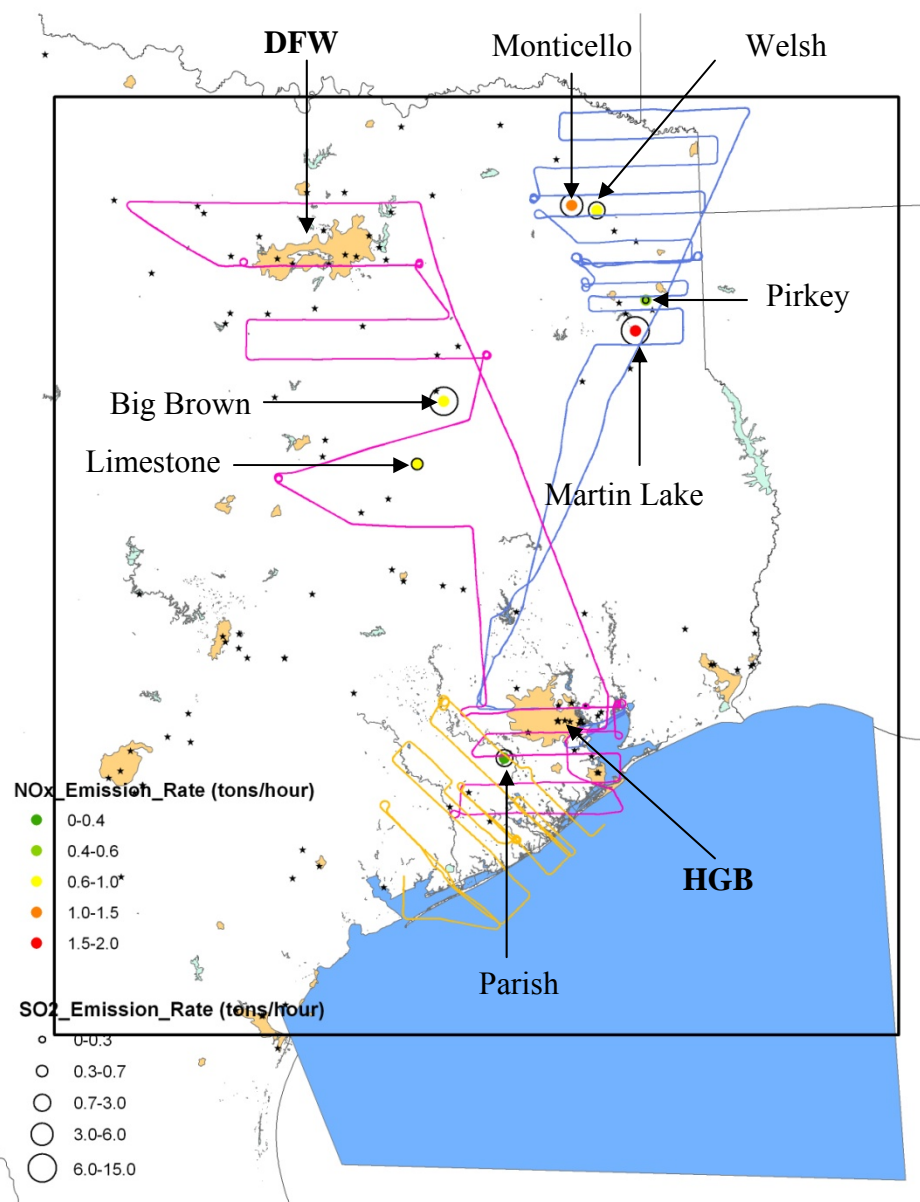


Fig. 1. WP-3 flight tracks (16 September in blue, 19 September in yellow, and 25 September in pink,) and power plants in eastern Texas. NO<sub>x</sub> emission rates are shown by colors and SO<sub>2</sub> emission rates are indicated by size of circles. Rectangular frame shows the 4km modeling domain. Black stars are all other point sources in Texas. The Houston-Galveston-Brazoria (HGB) and Dallas-Forth-Worth (DFW) metropolitan areas are also shown.

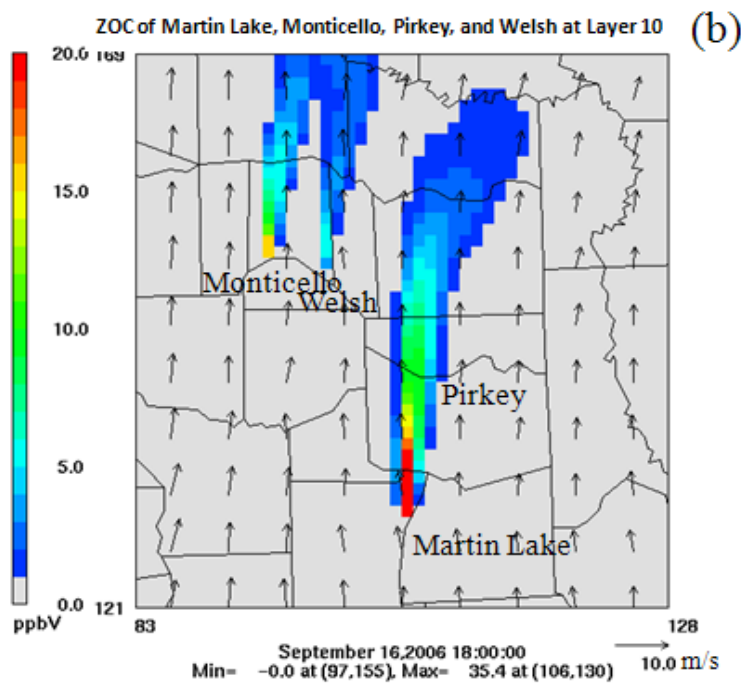
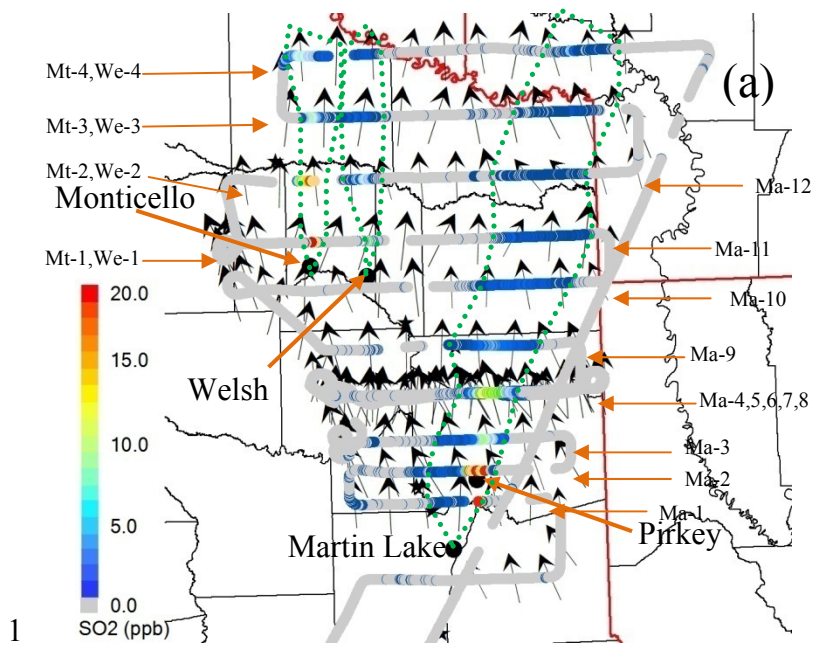


Fig. 2. (a) Observed PPPs of Martin Lake, Monticello, Pirkey, and Welsh on 16 September, 2006. The black dots show the locations of the power plants. PPPs are identified by measured  $\text{SO}_2$  enhancement (color gradient in the figure), as outlined by the green dash lines. Measured wind vectors are presented on the plume transect. The geographical redlines are the state boarder-lines. (b) Simulated PPPs of Martin Lake, Monticello, Pirkey, and Welsh at 18:00 GMT (600~700 m) (local time: 12:00)

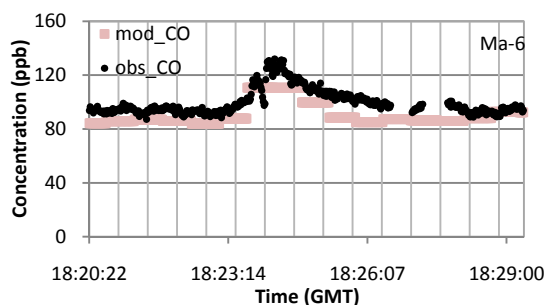
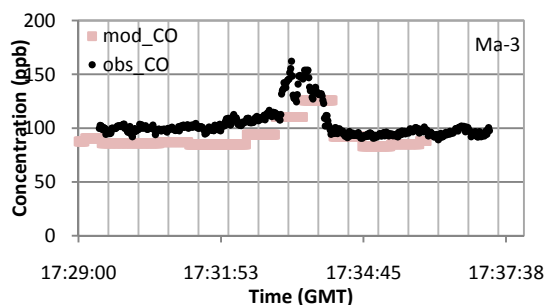
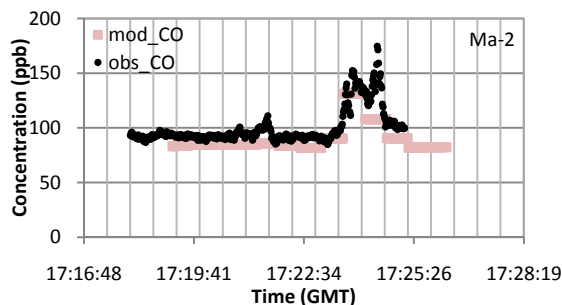
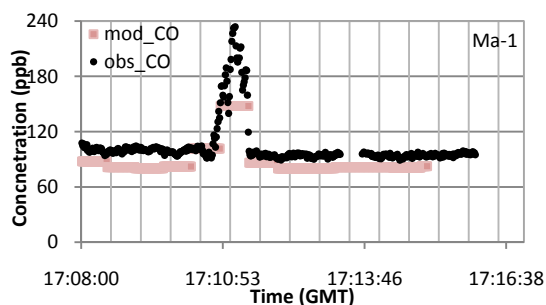
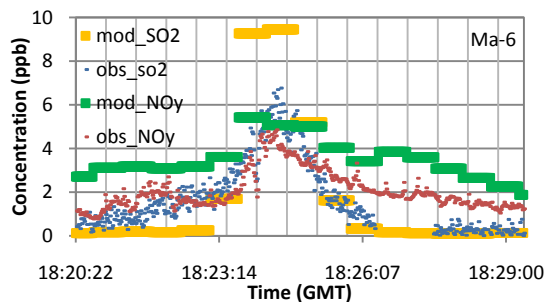
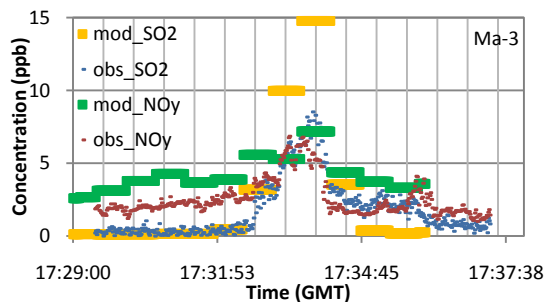
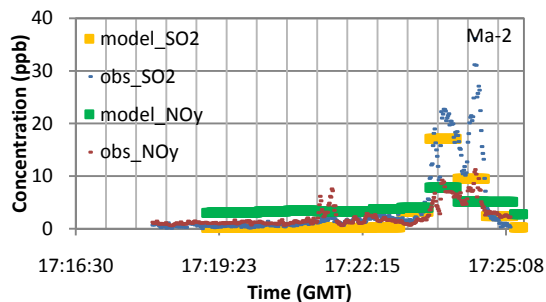
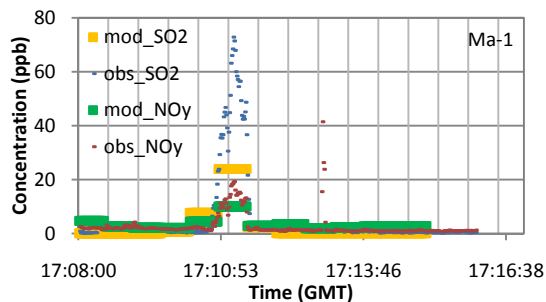


Fig. 3. The comparison of the modeled and observed  $\text{SO}_2$ ,  $\text{NO}_y$ , and  $\text{CO}$  at plume transect of Ma-1, Ma-2, Ma-3 and Ma-6. The modeled  $\text{SO}_2$ ,  $\text{NO}_y$ , and  $\text{CO}$  are labeled as yellow, green, and purple flat lines, respectively. The observed  $\text{SO}_2$ ,  $\text{NO}_y$ , and  $\text{CO}$  are labeled as blue, red and black dots. The Horizontal coordinate is time scale in GMT (local time = GMT - 6 hours) and vertical coordinate is concentration (ppb). Transect names listed in Table S3 of the manuscript are labeled in each subplot. Fig. S1-S4 summarize the comparisons for all the plume transects

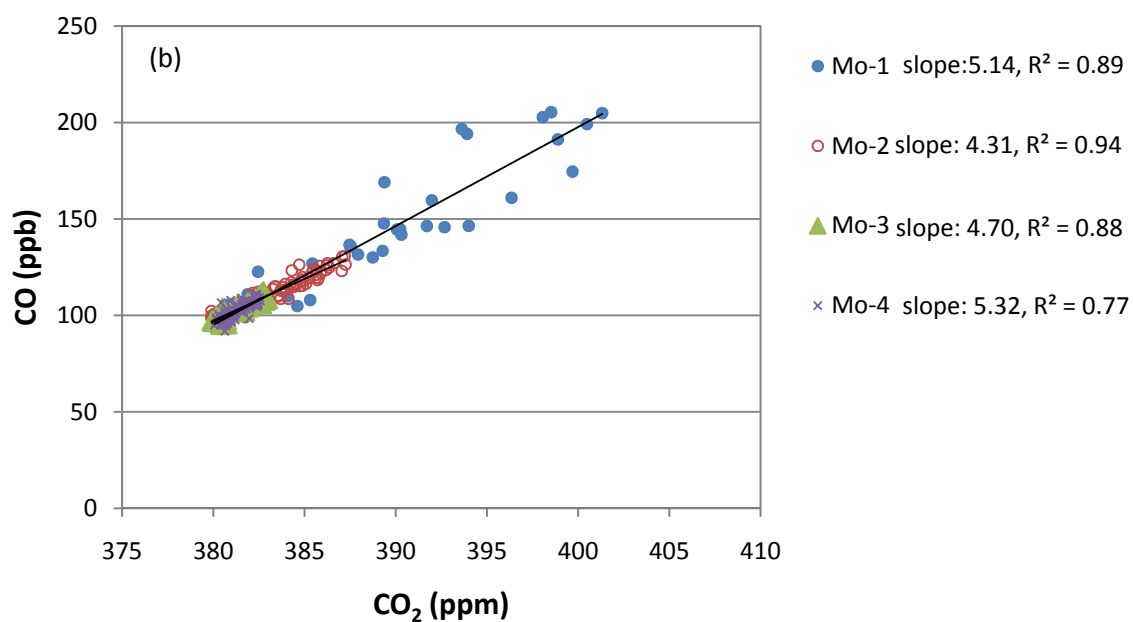
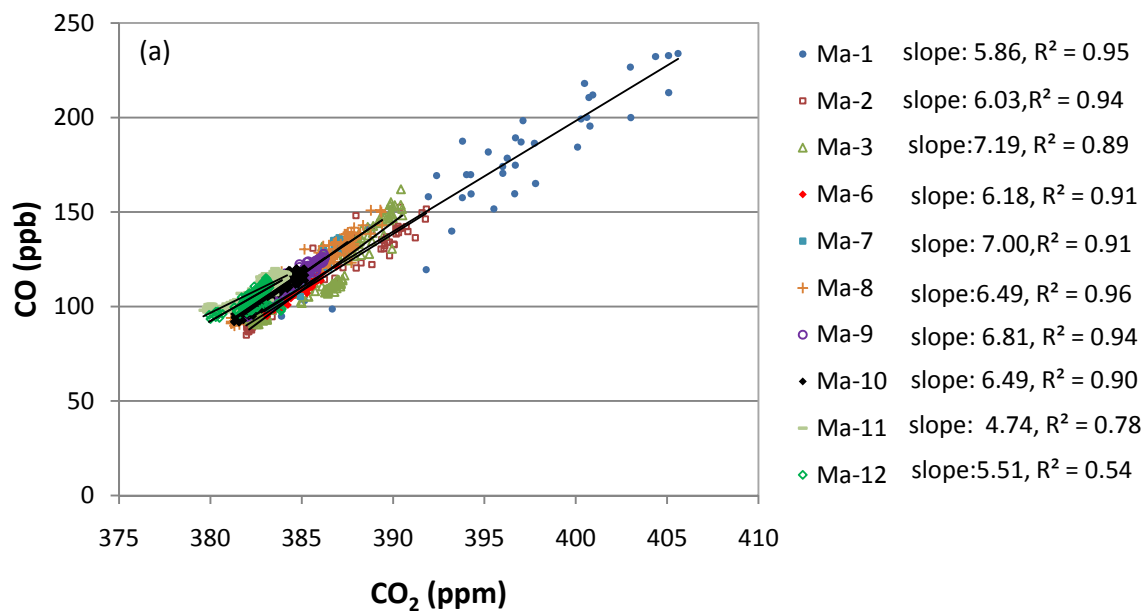


Fig. 4. Scatter plot of CO (ppb) versus CO<sub>2</sub> (ppm) from plume transects (a) Martin Lake (Ma-1 to Ma-12), and (b) Monticello (Mo-1 to Mo-4). The unit of the slopes from the least square fits is ppb/ppm.

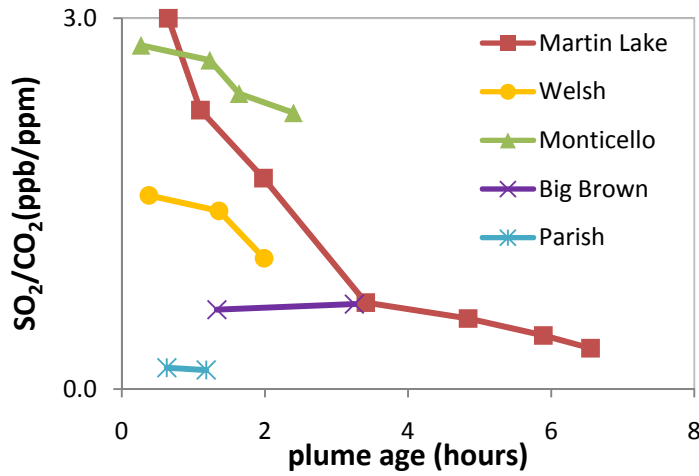
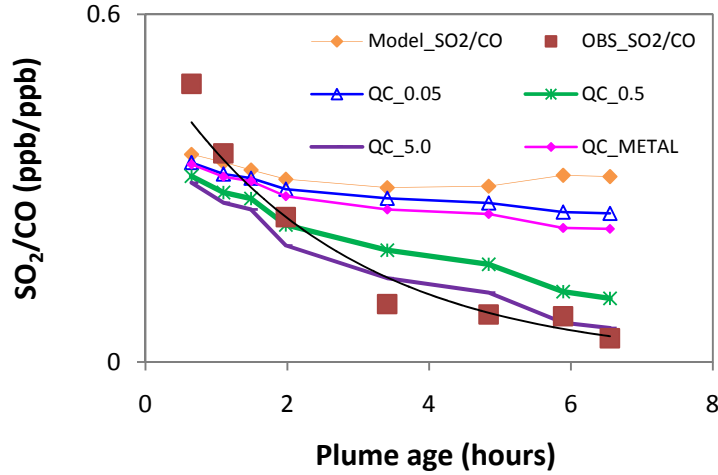


Fig. 5. (a) The observed least square slopes of  $\text{SO}_2$  to  $\text{CO}$  (red square) and modeled  $\text{ZOC}_{\text{SO}_2}/\text{ZOC}_{\text{CO}}$  (blue diamond for the base case, green dot for the adjusted cloud case) as a function of plume age at each transect of the Martin Lake plume (16 September). The observed  $\text{SO}_2$  loss rate was  $0.38 \text{ hour}^{-1}$  ( $R^2=0.94$ ,  $\text{SO}_2$  lifetime: 2.6 hours); the modeled  $\text{SO}_2$  loss rate was  $0.016 \text{ hour}^{-1}$  ( $R^2=0.36$ ,  $\text{SO}_2$  lifetime: 62.5 hours). The  $\text{SO}_2$  to  $\text{CO}$  slopes for each perturbation case are also plotted accordingly. (b) The observed least square slopes of  $\text{SO}_2$  to  $\text{CO}_2$  (ppb/ppm) for the five plumes; Martin Lake, Welsh, and Monticello plumes were observed on September 16 (cloudy day), Big Brown and Parish plumes were made on 25 September (sunny day).

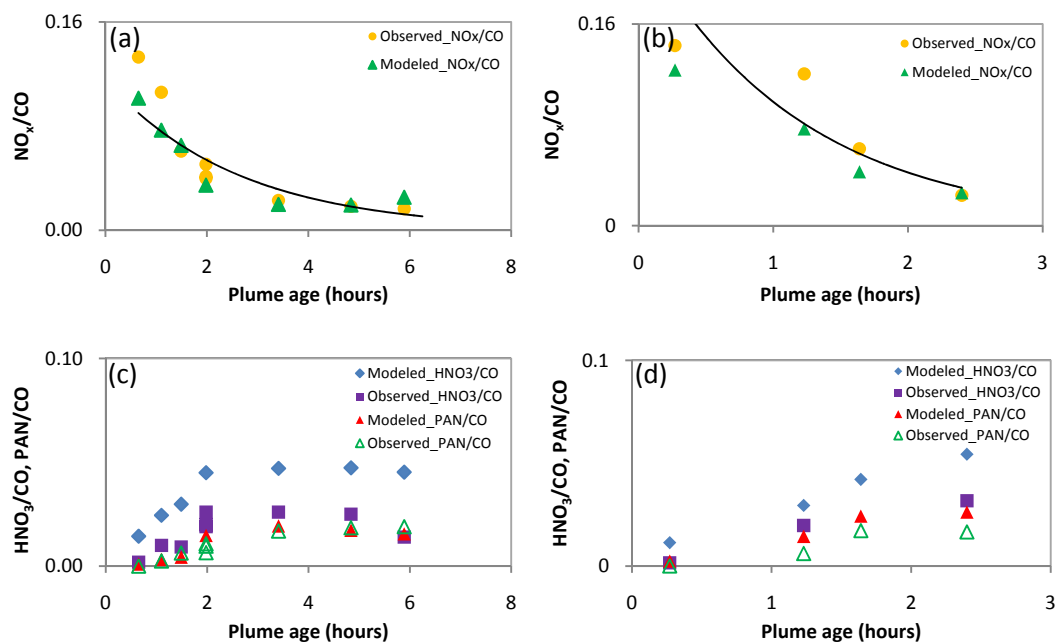


Fig. 6. Observed (yellow circle) and modeled (green triangle)  $\text{NO}_x/\text{CO}$  (a) for the Martin Lake plume, (b) for the Monticello plume. The observed  $\text{NO}_x$  oxidation rate was  $0.38 \text{ hour}^{-1}$  ( $R^2=0.85$ ) for the Martin Lake plume and  $0.84 \text{ hour}^{-1}$  ( $R^2=0.86$ ) for the Monticello plume. Observed and modeled  $\text{PAN}/\text{CO}$  and  $\text{HNO}_3/\text{CO}$ , (c) for the Martin Lake plume, (d) for the Monticello plume.

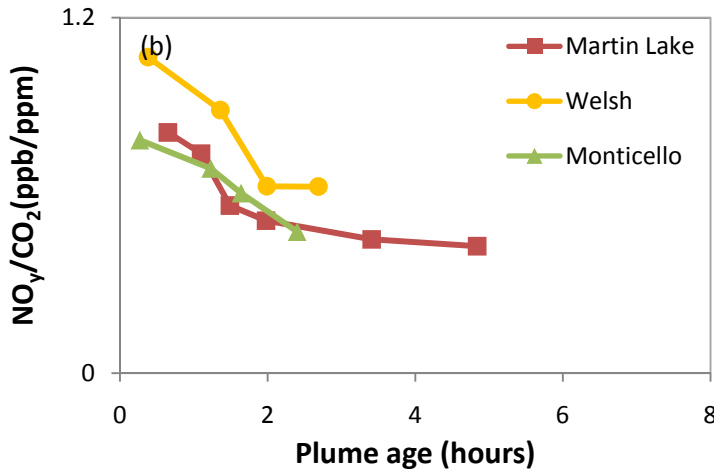
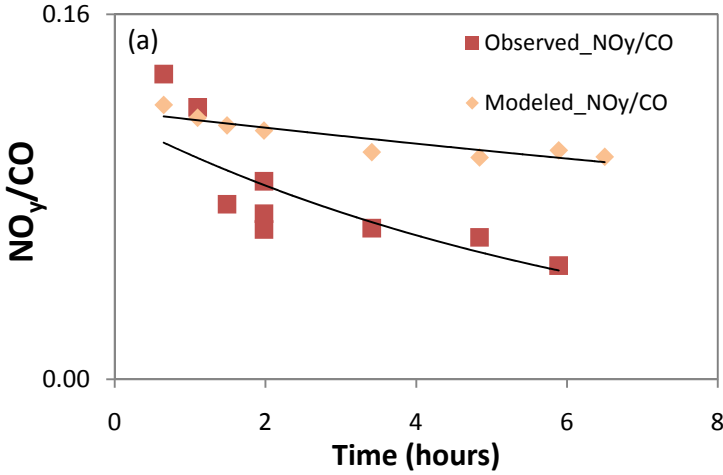


Fig. 7. (a) The observed least square slopes of  $\text{NO}_y$  to CO (red square) and modeled  $\text{ZOC}_{\text{NO}_y}/\text{ZOC}_{\text{CO}}$  (orange diamond for the base case, green dot for the adjusted cloud case) as a function of plume age at each transect of the Martin Lake plume; the observed  $\text{NO}_y$  loss rate was  $0.145 \text{ hour}^{-1}$  ( $R^2=0.69$ ) and the modeled  $\text{NO}_y$  loss rate was  $0.026 \text{ hour}^{-1}$  ( $R^2=0.48$ ). (b) The observed least square slopes of  $\text{NO}_y$  to  $\text{CO}_2$  (ppb/ppm) for the Martin Lake, Monticello, and Welsh.  $\text{NO}_y$  in the least-square fits was directly measured and not the sum of measured reactive nitrogen species.

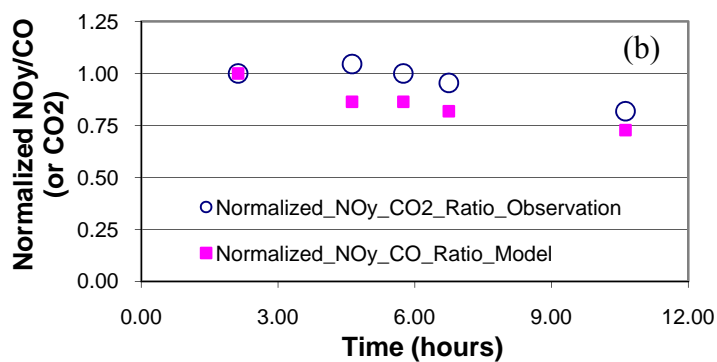
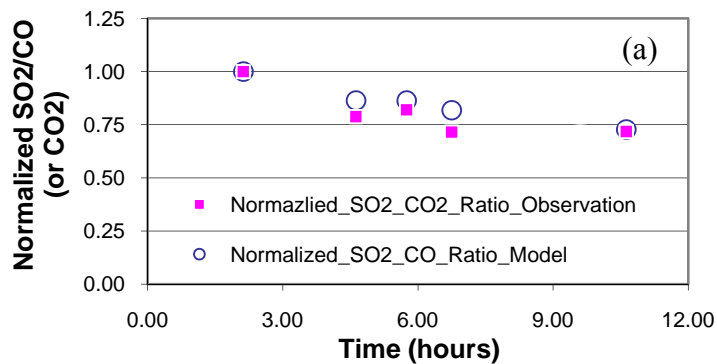
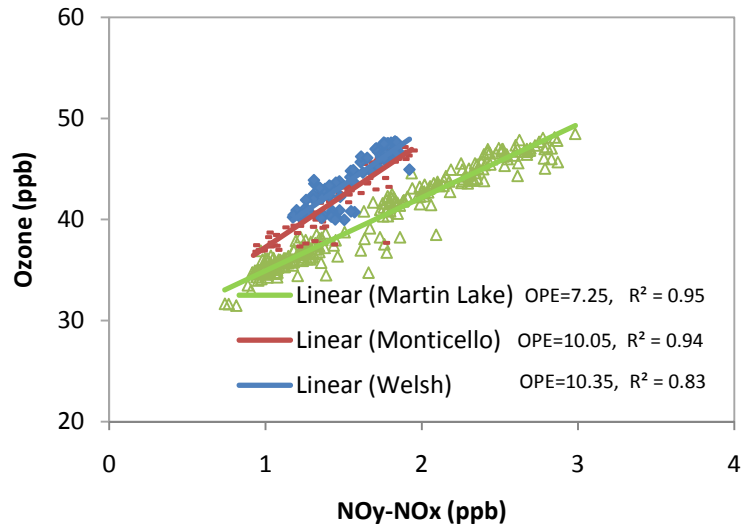


Fig. 8. The least-square-fit slopes of SO<sub>2</sub> to CO<sub>2</sub> (from the observation) and SO<sub>2</sub> to CO (from the model) (a), and the least-square-fit slopes of NO<sub>y</sub> to CO<sub>2</sub> (from the observation) and NO<sub>y</sub> to CO (from the observation) (b). All slopes are normalized to the slope at the first transect.



1  
2 Fig. 9. O<sub>3</sub> versus NO<sub>y</sub>-NO<sub>x</sub> from the transects of Martin Lake (Ma-6, plume age of 2.0 hours),  
3 Monticello (Mo-4, plume age of 2.4 hours), and Welsh (We-4, plume age of 2.7 hours). The  
4 slopes from the least square fits indicate the observation-based estimates of OPE from each  
5 plume transect.